Available online at www.sciencedirect.com
SCIENCE DIRECT®
Journal of Sound and Vibration 290 (2006) 736–762
JOURNAL OF SOUND AND VIBRATION
www.elsevier.com/locate/jsvi

Chaotic vibrations of circular cylindrical shells: Galerkin versus reduced-order models via the proper orthogonal decomposition method

M. Amabili[a,*], A. Sarkar[b], M.P. Païdoussis[c]

[a]*Dipartimento di Ingegneria Industriale, Università di Parma, Parco Area delle Scienze 181/A, Parma 43100, Italy*
[b]*School of Engineering, Carleton University, Ottawa, Ontario, Canada*
[c]*Department of Mechanical Engineering, McGill University, 817 Sherbrooke Street W., Montreal, Québec, Canada H3A 2K6*

Received 17 September 2004; received in revised form 10 March 2005; accepted 22 April 2005
Available online 8 September 2005

Abstract

The geometric nonlinear response of a water-filled, simply supported circular cylindrical shell to harmonic excitation in the spectral neighbourhood of the fundamental natural frequency is investigated. The response is investigated for a fixed excitation frequency by using the excitation amplitude as bifurcation parameter for a wide range of variation. Bifurcation diagrams of Poincaré maps obtained from direct time integration and calculation of the Lyapunov exponents and Lyapunov dimension have been used to study the system. By increasing the excitation amplitude, the response undergoes (i) a period-doubling bifurcation, (ii) subharmonic response, (iii) quasi-periodic response and (iv) chaotic behaviour with up to 16 positive Lyapunov exponents (hyperchaos). The model is based on Donnell's nonlinear shallow-shell theory, and the reference solution is obtained by the Galerkin method. The proper orthogonal decomposition (POD) method is used to extract proper orthogonal modes that describe the system behaviour from time-series response data. These time-series have been obtained via the conventional Galerkin approach (using normal modes as a projection basis) with an accurate model involving 16 degrees of freedom (dofs), validated in previous studies. The POD method, in conjunction with the Galerkin approach, permits to build a lower-dimensional model as compared to those obtainable via the conventional Galerkin approach. Periodic and quasi-periodic response around the fundamental resonance

*Corresponding author. Tel.: +39 0521 905 896; fax: +39 0521 905 705.
E-mail address: marco@me.unipr.it (M. Amabili).
URL: http://me.unipr.it/mam/amabili/amabili.html.

0022-460X/$ - see front matter
doi:10.1016/j.jsv.2005.04.034

for fixed excitation amplitude, can be very successfully simulated with a 3-dof reduced-order model. However, in the case of large variation of the excitation, even a 5-dof reduced-order model is not fully accurate. Results show that the POD methodology is not as "robust" as the Galerkin method.

1. Introduction

A very extensive literature review of work on the nonlinear dynamics of shells in vacuo, filled with or surrounded by quiescent or flowing fluids, is given by Amabili and Païdoussis [1]. From this review, it emerges that the choice of appropriate expressions for shell displacements is fundamental to guaranteeing accurate results of models for nonlinear (large-amplitude) vibrations of circular cylindrical shells. It is possible to attribute to Evensen [2] and Dowell and Ventres [3] the original idea of modal expansions of the shell flexural displacement involving (i) two asymmetric modes with the same shape (sine and cosine functions around the shell circumference: one directly driven by external excitation, the driven mode; the other, normally referred to as the companion mode) and (ii) an axisymmetric term; this intuitive assumption was supported by the few available experimental results.

In a recent series of papers, Amabili et al. [4–7] systematically studied the nonlinear dynamics and large-amplitude vibrations of simply supported, circular cylindrical shells, with and without quiescent or flowing fluid, by using as a basis the natural modes. In particular, the convergence of the solution was studied in Refs. [5,6]. Amabili [8] investigated the effect of geometric imperfections and compared calculations and experiments by validating the theory. More accurate shell theories have been used by Amabili [9] to study the same problem. Results show that, for water-filled shells, Donnell's nonlinear shallow-shell theory gives reasonably accurate results.

In the present study, the nonlinear (large-amplitude) response of simply supported circular cylindrical shells to harmonic excitation in the spectral neighbourhood of the fundamental natural frequency is investigated. The shell is assumed to be completely filled with an incompressible and inviscid fluid at rest. Donnell's nonlinear shallow-shell theory is used, and the solution is obtained by the Galerkin method. The response is investigated for a fixed excitation frequency by using the excitation amplitude as bifurcation parameter over a wide range of variation. Bifurcation diagrams of Poincaré maps obtained from direct time integration and calculation of the maximum Lyapunov exponent have been used to study the system. By increasing the excitation amplitude, the response undergoes (i) period-doubling bifurcation, (ii) subharmonic response, (iii) quasi-periodic response and (iv) chaotic behavior (hyperchaos). The proper orthogonal decomposition (POD) method, also referred to as the Karhunen–Loève method [10–16], is used to extract proper orthogonal modes (POM) from the system time response, in order to describe the shell behaviour with a low-dimensional model. The shell time responses have initially been obtained by a conventional Galerkin approach with an accurate model involving 16 degrees of freedom (dofs), previously developed by Amabili for periodic response [8]. Then, two different reduced models have been developed from POM extracted from time series for quasi-periodic and chaotic responses.

Recently, Amabili et al. [17] have shown that periodic and quasi-periodic response around the fundamental resonance for a fixed excitation (relatively small) amplitude can be very successfully calculated with a 3-dof reduced-order model, but great care must be taken in the selection of time responses used to extract the POD modes. The present study shows that, in the case of extremely large variation of a system parameter (force magnitude in this case) and very complex system dynamics (period-doubling bifurcation, chaos, hyperchaos), even a 5-dof reduced-order model, built from chaotic time series, is not fully accurate. Modes extracted from chaotic time series by using POD have recently been discussed by Kerschen et al. [16]. They have shown that, for a clamped beam, modes extracted from chaotic response are more representative of the system dynamics than any other set of modes extracted from a non-chaotic response. In the present paper, some further discussion on this issue is given for a more complex system. As the present model has already been presented in Ref. [17], some details are skipped in this paper to avoid repetition.

2. Basic equations and conventional Galerkin solution

A cylindrical coordinate system (O; x, r, θ) is chosen, with the origin O placed at the centre of one end of the shell. The displacements of the shell middle surface are denoted by u, v and w, in the axial, circumferential and radial directions, respectively; w is taken positive inwards, as shown in Fig. 1. Initial imperfections of the circular cylindrical shell associated with zero initial tension are denoted by an inward radial displacement w_0; only radial initial imperfections are considered. By using Donnell's nonlinear shallow-shell theory, the equation of motion for finite-amplitude transverse deflection is given by [3,8]

$$D\nabla^4 w + ch\dot{w} + \rho h\ddot{w} = f - p + \frac{1}{R}\frac{\partial^2 F}{\partial x^2} + \frac{1}{R^2}\left[\frac{\partial^2 F}{\partial \theta^2}\left(\frac{\partial^2 w}{\partial x^2} + \frac{\partial^2 w_0}{\partial x^2}\right) - 2\frac{\partial^2 F}{\partial x \partial \theta}\left(\frac{\partial^2 w}{\partial x \partial \theta} + \frac{\partial^2 w_0}{\partial x \partial \theta}\right) + \frac{\partial^2 F}{\partial x^2}\left(\frac{\partial^2 w}{\partial \theta^2} + \frac{\partial^2 w_0}{\partial \theta^2}\right)\right], \tag{1}$$

where $D = Eh^3/[12(1-\nu^2)]$ is the flexural rigidity, E Young's modulus, ν the Poisson ratio, h the shell thickness, R the mean shell radius, ρ the mass density of the shell, c the coefficient of viscous

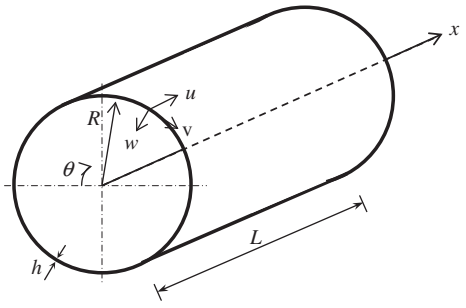

Fig. 1. Shell geometry and coordinate system.

damping, p the radial pressure applied to the surface of the shell by the contained fluid, and f is an external local excitation:

$$f = \tilde{f}\delta(R\theta - R\tilde{\theta})\delta(x - \tilde{x})\cos(\omega t), \tag{2}$$

where δ is the Dirac delta function, $\tilde{f}$ is the magnitude of the localized (point) force, and $\tilde{\theta}$ and $\tilde{x}$ give the angular and axial coordinates of the point of application of the force, respectively. Excitations with frequency close to the natural frequency of the lowest modes of the shell are considered; low-frequency modes are associated with predominantly radial motion and are identified by the pair (m, n), where m is the number of axial half-waves and n is the number of circumferential waves. The viscous damping model introduced in Eq. (1) is unrealistic; it will later be replaced by modal damping coefficients, experimentally identified, in the equations of motion.

In Eq. (1), the overdot denotes a time derivative, and F is the in-plane Airy stress function, which is given by the following compatibility equation [3,8]:

$$\frac{1}{Eh}\nabla^4 F = -\frac{1}{R}\frac{\partial^2 w}{\partial x^2} + \frac{1}{R^2}\left[\left(\frac{\partial^2 w}{\partial x \partial \theta}\right)^2 + 2\frac{\partial^2 w}{\partial x \partial \theta}\frac{\partial^2 w_0}{\partial x \partial \theta} - \left(\frac{\partial^2 w}{\partial x^2} + \frac{\partial^2 w_0}{\partial x^2}\right)\frac{\partial^2 w}{\partial \theta^2} - \frac{\partial^2 w}{\partial x^2}\frac{\partial^2 w_0}{\partial \theta^2}\right]. \tag{3}$$

In Eqs. (1) and (3), the biharmonic operator is defined as $\nabla^4 = [\partial^2/\partial x^2 + \partial^2/(R^2\partial\theta^2)]^2$. Donnell's nonlinear shallow-shell equations are accurate only for modes with a large number n of circumferential waves; it is generally assumed that $1/n^2 \ll 1$ is required in order to have fairly good accuracy (i.e. $n \geqslant 4$). Donnell's nonlinear shallow-shell equations are obtained by neglecting the in-plane inertia, transverse shear deformation and rotary inertia, giving accurate results only for thin shells. In-plane displacements are assumed to be infinitesimal, whereas w is of the same order as the shell thickness. The accuracy of this shell theory has been discussed by Amabili [9].

The forces per unit length in the axial and circumferential directions, as well as the shear force, are given by [3]

$$N_x = \frac{1}{R^2}\frac{\partial^2 F}{\partial \theta^2}, \quad N_\theta = \frac{\partial^2 F}{\partial x^2}, \quad N_{x\theta} = -\frac{1}{R}\frac{\partial^2 F}{\partial x \partial \theta}. \tag{4}$$

The force–displacement relations are [8]:

$$(1-\nu^2)\frac{N_x}{Eh} = -\frac{\nu w}{R} + \frac{1}{2}\left(\frac{\partial w}{\partial x}\right)^2 + \frac{\partial w}{\partial x}\frac{\partial w_0}{\partial x} + \frac{\nu}{2}\left(\frac{\partial w}{R\partial \theta}\right)^2 + \nu\frac{\partial w}{R\partial\theta}\frac{\partial w_0}{R\partial\theta} + \frac{\partial u}{\partial x} + \frac{\nu}{R}\frac{\partial v}{\partial \theta}, \tag{5}$$

$$(1-\nu^2)\frac{N_\theta}{Eh} = -\frac{w}{R} + \frac{\nu}{2}\left(\frac{\partial w}{\partial x}\right)^2 + \nu\frac{\partial w}{\partial x}\frac{\partial w_0}{\partial x} + \frac{1}{2}\left(\frac{\partial w}{R\partial \theta}\right)^2 + \frac{\partial w}{R\partial\theta}\frac{\partial w_0}{R\partial\theta} + \nu\frac{\partial u}{\partial x} + \frac{1}{R}\frac{\partial v}{\partial \theta}, \tag{6}$$

$$(1-\nu^2)\frac{N_{x\theta}}{Eh} = 2(1-\nu)\left[\frac{1}{R}\frac{\partial w}{\partial x}\frac{\partial w}{\partial \theta} + \frac{1}{R}\frac{\partial w}{\partial x}\frac{\partial w_0}{\partial \theta} + \frac{1}{R}\frac{\partial w_0}{\partial x}\frac{\partial w}{\partial \theta} + \frac{1}{R}\frac{\partial u}{\partial \theta} + \frac{\partial v}{\partial x}\right], \tag{7}$$

where $w_0(x, \theta)$ is the assumed radial imperfection in the shell.

In this study, attention is focused on simply supported, circumferentially closed circular cylindrical shells of length L. The following out-of-plane (shell surface) boundary conditions are imposed:

$$w = w_0 = 0, \tag{8a}$$

$$M_x = -D\{(\partial^2 w/\partial x^2) + \nu[\partial^2 w/(R^2\partial\theta^2)]\} = 0 \tag{8b}$$

and

$$\partial^2 w_0/\partial x^2 = 0, \quad \text{at } x = 0, L, \tag{8c}$$

where M_x is the bending moment per unit length. The in-plane boundary conditions are

$$N_x = 0 \quad \text{and} \quad v = 0 \ \text{ at } x = 0, L. \tag{9a,b}$$

Moreover, u, v and w must be continuous in θ.

2.1. Modal expansion and equation of motion

Previous studies have shown that a linear modal base is the simplest choice for discretizing the shell [4–8]. In particular, in order to reduce the number of dofs, it is important to use only the most significant modes. In addition to the asymmetric mode directly driven into vibration by the excitation (driven mode), it is necessary to consider (i) the orthogonal mode having the same shape and natural frequency but rotated by $\pi/(2n)$ (companion mode), (ii) additional asymmetric modes, and (iii) axisymmetric modes. In fact, it has clearly been established that, for large-amplitude shell vibrations, the deformation of the shell involves significant axisymmetric oscillations inwards. According to these considerations, the radial displacement w is expanded by using the eigenmodes of the empty shell, which are unchanged for the completely filled shell [8]:

$$w(x,\theta,t) = \sum_{m=1}^{3}\sum_{k=1}^{3}\left[A_{m,kn}(t)\cos(kn\theta) + B_{m,kn}(t)\sin(kn\theta)\right]\sin(\lambda_m x) + \sum_{m=1}^{4} A_{(2m-1),0}(t)\sin(\lambda_{(2m-1)}x), \tag{10a}$$

where n is the number of circumferential waves, m is the number of longitudinal half-waves (only odd values are used for symmetry), $\lambda_m = m\pi/L$, and t is the time; $A_{m,n}(t)$, $B_{m,n}(t)$ and $A_{m,0}(t)$ are the generalized coordinates that are unknown functions of t. The number of dofs used in the present numerical calculations is 16.

The presence of pairs of modes having the same shape but different angular orientations, the first one described by $\cos(n\theta)$ (driven mode for the excitation given by Eq. (2)) and the other by $\sin(n\theta)$ (companion mode), in the periodic response of the shell leads to the appearance of a travelling wave around the shell in the azimuthal direction when both these modes are active and when they have a relative time shift. This phenomenon is related to the axial symmetry of the system.

When the excitation has a frequency close to the resonance of a particular mode, say ($m = 1$, n), results for relatively low amplitude excitation (case of periodic response) show that (i) the generalized coordinates $A_{1,n}(t)$ and $B_{1,n}(t)$ have the same frequency as the excitation, (ii) the coordinates $A_{1,2n}(t)$, $B_{1,2n}(t)$, $A_{3,2n}(t)$, $B_{3,2n}(t)$ and all the coordinates associated with axisymmetric modes have twice the frequency of the excitation, and (iii) the coordinates $A_{3,n}(t)$, $B_{3,n}(t)$, $A_{1,3n}(t)$, $B_{1,3n}(t)$, $A_{3,3n}(t)$ and $B_{3,3n}(t)$ have three times the frequency of the excitation.

In order to simplify the notation, Eq. (10a) is re-written in the following compact form:

$$w(x,\theta,t)=\sum_{m=1}^{M}\sum_{n=0}^{N}\left[A_{m,n}(t)\,\cos(n\theta)+B_{m,n}(t)\,\sin(n\theta)\right]\,\sin(\lambda_m x), \tag{10b}$$

where M and N are integers indicating the number of terms used in this expansion.

The initial radial imperfection w_0 is expanded in the same form of w, i.e. in a double Fourier series satisfying boundary conditions (8a,c) at the shell edges,

$$w_0(x,\theta)=\sum_{m=1}^{\tilde{M}}\sum_{n=0}^{\tilde{N}}\left[\tilde{A}_{m,n}\,\cos(n\theta)+\tilde{B}_{m,n}\,\sin(n\theta)\right]\,\sin(\lambda_m x), \tag{11}$$

where $\tilde{A}_{m,n}$ and $\tilde{B}_{m,n}$ are the modal amplitudes of the imperfections; $\tilde{N}$ and $\tilde{M}$ indicate the number of terms in the expansion.

Expansion (10) used for the radial displacement w satisfies identically the boundary conditions given by Eqs. (8a) and (8b); moreover, it satisfies exactly the continuity of the circumferential displacement. The boundary conditions for the in-plane displacements, Eqs. (9a,b), give very complex expressions when transformed into equations involving w. Therefore, they are modified into simpler integral expressions that satisfy Eqs. (9a,b) *on the average* [3,4].

When the expansions of w and w_0, Eqs. (10) and (11), are substituted in the right-hand side of Eq. (3), a partial differential equation for the stress function F is obtained, composed of the homogeneous and the particular solution.

By use of the Galerkin method, 16 second-order, ordinary, coupled nonlinear differential equations are obtained for the variables $A_{m,kn}(t)$, $B_{m,kn}(t)$ and $A_{m,0}(t)$, for $m=1,\ldots,M$ and $k=1,\ldots,3$, by successively weighting the original Eq. (1) with the functions that describe the shape of the modes retained in Eq. (10). These equations have very long expressions containing quadratic and cubic nonlinear terms.

The equations of motion have been obtained by using the *Mathematica 4* computer software [18], in order to perform analytical integrals of trigonometric functions. The generic jth Lagrange equation is divided by the modal mass associated with $\ddot{q}_j$ and is then transformed into the following two first-order equations by using the dummy variable y_j:

$$\begin{aligned}
&\dot{q}_j = y_j,\\
&\dot{y}_j = -2\zeta_j\omega_j y_j-\sum_{i=1}^{\text{dofs}} z_{j,i}q_i-\sum_{i=1}^{\text{dofs}}\sum_{k=1}^{\text{dofs}} z_{j,i,k}q_iq_k-\sum_{i=1}^{\text{dofs}}\sum_{k=1}^{\text{dofs}}\sum_{l=1}^{\text{dofs}} z_{j,i,k,l}q_iq_kq_l+f\cos(\omega t)\\
&\qquad \text{for } j=1,\ldots,\text{dofs},
\end{aligned} \tag{12}$$

where $f=0$ if $q_j=B_{m,n}$ and coefficients z have long expressions that include also geometric imperfections. In Eq. (12), each generalized coordinate q_j (and therefore the modal damping ζ_j and circular frequency ω_j) has to be referred to mode (m,n), i.e. $q_j=A_{m,n}$ or $B_{m,n}$. For computational convenience a non-dimensionalization of variables is also performed: the time is divided by the period of the resonant mode and the vibration amplitudes are divided by the shell thickness h. The resulting $2\times$ dofs first-order nonlinear differential equations are studied by using (i) the software AUTO 97 [19] for continuation and bifurcation analysis of nonlinear ordinary differential equations, and (ii) direct integration of the equations of motion by using the DIVPAG

routine of the Fortran library IMSL. Continuation methods allow following the solution path, with the advantage that unstable solutions can also be obtained; these are not ordinarily attainable by using direct numerical integration. The software AUTO 97 is capable of continuation of the solution, bifurcation analysis and branch switching by using arclength continuation and collocation methods. In particular, the shell response under harmonic excitation has been studied by using an analysis in two steps: (i) first the excitation frequency has been fixed far enough from resonance and the magnitude of the excitation has been used as bifurcation parameter; the solution has been started at zero force (where the solution is the trivial undisturbed configuration of the shell) and it has been continued upwards to reach the desired force magnitude; (ii) when the desired magnitude of excitation has been reached, the solution was continued by using the excitation frequency as bifurcation parameter.

Direct integration of the equations of motion by using Gear's BDF method (routine DIVPAG of the Fortran library IMSL) has also been performed, when specified in the following sections, to check the results and obtain the time behaviour. The Adams–Gear algorithm was used due to the relatively high dimension of the dynamical system. Indeed, when a high-dimensional phase space is analyzed, the problem can display stiff numerical characteristics, due to the presence of different time scales in the response. In fact, in simulations with adaptive step-size Runge–Kutta methods, spurious non-stationary and divergent motions can be obtained.

The bifurcation diagram of the Poincaré maps was used in case of non-stationary response, i.e. to analyze a wide range of excitation magnitudes where the shell response changes dramatically. This bifurcation diagram has been constructed by using the time integration scheme and by varying the force amplitude.

2.2. Maximum Lyapunov exponent

In order to evaluate the maximum Lyapunov exponent, which is useful to characterize regular or chaotic motion of the shell, it is necessary to assume a reference trajectory $\mathbf{x}_r(t)$ in the phase plane ($\mathbf{q}$, $\dot{\mathbf{q}}$ plane) and observe a neighbouring trajectory originated at infinitesimal initial perturbation $\delta\mathbf{x}(t_0)$ from the reference trajectory (see Ref. [20]). The evolution of the perturbation during time, $\delta\mathbf{x}(t)$, is governed by the following variational equations directly obtained from Eq. (12):

$$\begin{aligned}
&\frac{\mathrm{d}}{\mathrm{d}t}\delta q_j = \delta y_j\\
&\frac{\mathrm{d}}{\mathrm{d}t}\delta y_j = -2\zeta_j\omega_j\delta y_j - \sum_{i=1}^{\mathrm{dofs}} z_{j,i}\delta q_i - \sum_{n=1}^{\mathrm{dofs}}\sum_{i=1}^{\mathrm{dofs}}\sum_{k=1}^{\mathrm{dofs}} z_{j,i,k}\delta q_n\left(\delta_{k,n}q_i + \delta_{i,n}q_k\right)\\
&\qquad - \sum_{n=1}^{\mathrm{dofs}}\sum_{i=1}^{\mathrm{dofs}}\sum_{k=1}^{\mathrm{dofs}}\sum_{l=1}^{\mathrm{dofs}} z_{j,i,k,l}\,\delta q_n\left(\delta_{i,n}q_k q_l + \delta_{k,n}q_i q_l + \delta_{l,n}q_k q_i\right), \quad \text{for } j = 1,\ldots,\mathrm{dofs},
\end{aligned} \tag{13}$$

where $\delta_{k,n}$ is the Kronecker delta. Taking δq_j and δy_j as new variables, the simultaneous integration of the $4\times\mathrm{dofs}$ first-order differential equations has been performed (Eqs. (12) are nonlinear and is integrated by using DIVPAG IMSL routine, and Eqs. (13) are linear, but with time-varying coefficients, and are integrated by using the adaptive step-size 4th/5th order

Runge–Kutta method). The excitation period has been divided into 10^4 integration steps Δt in order to have accurate evaluation of the time-varying coefficients in Eq. (13) that are obtained at each step by integration of Eq. (12). To find a reference trajectory, 5×10^6 steps are skipped in order to eliminate the transient and 1×10^6 steps are skipped to eliminate the transient in the variational Eq. (13). Then, 1×10^6 steps are used for evaluation of the maximum Lyapunov exponent σ_1 for the reference trajectory $\mathbf{x}_r(t)$, which is given by

$$\sigma_1 = \lim_{t\to\infty} \sup \frac{1}{t} \ln \frac{\left|\delta\mathbf{x}(t)\right|}{\left|\delta\mathbf{x}(t_0)\right|}. \tag{14}$$

Assuming an initial perturbation of unitary amplitude, Eq. (14) is simplified into

$$\sigma_1 = \lim_{t\to\infty} \sup \frac{1}{t} \ln\left|\delta\mathbf{x}(t).\right| \tag{15}$$

Then, by restoring at each integration time step k the amplitude of $\delta\mathbf{x}(t)$ to its original unitary measure by the re-normalization

$$\delta\bar{\mathbf{x}}(t)_k = \frac{\delta\mathbf{x}(t)_k}{d_k},$$

where $\left|\delta\mathbf{x}(t)\right|_k = d_k$, the following formula for the maximum Lyapunov exponent, evaluated at step k, is obtained

$$\sigma_{1,k} = \frac{1}{k\,\Delta t} \sum_{i=1}^{k} \ln\, d_i. \tag{16}$$

In the numerical calculation of the maximum Lyapunov exponent, the non-dimensional time previously introduced has been used. A perturbation vector $\mathbf{f}_1$ is determined with the maximum Lyapunov exponent σ_1.

2.3. All Lyapunov exponents

The Fortran computer program developed to calculate $2 \times$ dofs numbers designating the spectrum of the Lyapunov exponents [20] is described in Ref. [21] and has been properly validated. In particular, 1×10^7 steps have been used to evaluate the Lyapunov exponents (10 times larger than for calculation of the maximum Lyapunov exponent that has been evaluated for all the bifurcation diagrams, with high computational cost).

2.4. Lyapunov dimension

The long-term behaviour of dissipative systems is characterized by attractors of the most varied types if the trajectories are not drawn towards infinity. After a transient state, in which some modes of motion finally vanish due to damping, the state of the system approaches an attractor where the number of independent variables, which determine the dimension of the phase space, is generally reduced considerably [20]. The fractal dimension is a measure of the strangeness of an attractor and indicates the number of effective independent variables determining the long-term behaviour of a motion. There exist several measures of the fractal dimension, including the

well-known Lyapunov dimension, which is defined as [20]

$$d_L = s + \sum_{r=1}^{s} \sigma_r / |\sigma_{s+1}|, \tag{17}$$

where the Lyapunov exponents are ordered by their magnitude, and s is obtained by satisfying the following conditions:

$$\sum_{r=1}^{s} \sigma_r > 0 \quad \text{and} \quad \sum_{r=1}^{s+1} \sigma_r < 0.$$

2.5. Fluid–structure interaction

The contained fluid is assumed to be incompressible, inviscid and irrotational, so that potential theory can be used to describe fluid motion. Liquid-filled shells vibrating in the low-frequency range satisfy the incompressibility hypothesis very well. Nonlinear effects in the dynamic pressure and in the boundary conditions at the fluid–structure interface are neglected. The shell prestress due to the fluid weight is also neglected. The fluid motion is described by the velocity potential Φ, which satisfies the Laplace equation [4,8,22]. Cavitation is assumed not to occur at the fluid–shell interface. Both ends of the fluid volume (corresponding to the shell edges) are assumed to be open, so that a zero pressure is assumed there; this physically corresponds to a long shell periodically supported (e.g. with ring stiffeners) or it approximates a can closed by very thin circular plates. The dynamic pressure p exerted by the contained fluid on the shell is given by [8]

$$p = \rho_F \left(\dot{\Phi}\right)_{r=R} = \sum_{m=1}^{M} \sum_{n=1}^{N} \rho_F \left[\ddot{A}_{m,n}(t) \cos(n\theta) + \ddot{B}_{m,n}(t) \sin(n\theta)\right] \frac{\mathrm{I}_n(\lambda_m R)}{\lambda_m \mathrm{I}'_n(\lambda_m R)} \sin(\lambda_m x), \tag{18}$$

where ρ_F is the mass density of the internal fluid, I_n is the modified Bessel function of order n, and I'_n its derivative with respect to the argument. Eqs. (18) and (10) present the same spatial distribution on the shell surface. Therefore, fluid pressure gives only an inertial effect, which is different for each mode of the expansion. Hence, the fluid is expected to change the nonlinear behaviour of the fluid-filled shell, as a consequence of the fundamental interaction among asymmetric and the axisymmetric modes. Usually the inertial effect of the fluid is larger for axisymmetric modes, thus enhancing the nonlinear softening-type behaviour of the shell.

3. Galerkin solution with POD method

As discussed in the previous section, a Galerkin procedure, employing any set of basis functions φ_i, approximates the nonlinear PDE by transforming it into a finite set of coupled ordinary differential equations (ODEs), with the solution being expressed as

$$w(\xi, t) = \sum_{i=1}^{K} q_i(t)\, \varphi_i(\xi), \tag{19}$$

where t is the time, ξ is the vector of spatial coordinate (x, θ) describing the shell middle surface Ω, $q_i(t)$ are the generalized coordinates, and K is the number of degrees of freedom, i.e. the number of basis functions assumed. Next, the POM (also referred to as spatially coherent modes) obtained by the POD method will be used as a basis in conjunction with the Galerkin approach.

The POD method optimally extracts the spatial information necessary to characterize the spatio-temporal complexity and inherent dimension of a system, from a set of temporal snapshots of the response, gathered from either numerical simulations or experimental data [10–17]. In the present context, the temporal responses are obtained via the conventional Galerkin solution. It can be observed here that, for large-amplitude experimentally measured vibration, responses can be highly noise-polluted.

The solution can be expressed by using the basis of the POM $\psi_i(\xi)$,

$$w(\xi, t) = \sum_{i=1}^{\tilde{K}} a_i(t)\psi_i(\xi), \tag{20}$$

where a_i are the proper orthogonal coordinates and $\tilde{K}$ is the number of degrees of freedom of the POD solution (in general, significantly lower than K).

The displacement field w is divided into its time-mean value $\bar{w}(\xi)$ and the zero-mean response $\tilde{w}(\xi, t) = (w(\xi, t) - \bar{w}(\xi))$. In the POD method, the POM are obtained by minimizing the objective function

$$\tilde{\lambda} = \left\langle (\psi(\xi) - \tilde{w}(\xi, t))^2 \right\rangle \quad \forall \xi \in \Omega, \tag{21}$$

with $\langle\ \rangle$ denoting the time-averaging operation and $\psi(\xi)$ the generic POD mode. If the temporal snapshots of $\tilde{w}$ are denoted by $\{\tilde{w}_n\}$, the time-averaging operation of a series of N snapshots is $\left\langle \tilde{w}(\xi, t) \right\rangle = (1/N) \sum_{n=1}^{N} \tilde{w}_n(\xi)$. Minimizing of the objective function (21) is obtained, after some mathematics, by solving the following eigenvalue problem:

$$\int_{\Omega} \left\langle \tilde{w}(\xi, t)\tilde{w}(\xi', t) \right\rangle \psi(\xi')\xi' = \lambda\psi(\xi), \tag{22}$$

where $\langle \tilde{w}(\xi, t)\tilde{w}(\xi', t) \rangle$ is the time-averaged spatial autocorrelation function.

A Galerkin projection scheme for determining the POM semi-analytically [23], and in parallel to approximate the solution of the PDE, is presented next. The generic POM is projected on the eigenmodes $\varphi_i(\xi)$ of the empty shell as

$$\psi(\xi) = \sum_{i=1}^{K} \alpha_i \varphi_i(\xi), \tag{23}$$

where α_i are unknown coefficients. Then, the following eigenvalue problem is finally obtained:

$$\mathbf{A}\boldsymbol{\alpha} = \lambda \mathbf{B}\boldsymbol{\alpha}, \tag{24}$$

where

$$A_{ij} = \tau_i\tau_j \left\langle \tilde{q}_i(t)\, \tilde{q}_j(t) \right\rangle, \quad B_{ij} = \tau_i\delta_{ij}, \quad \tau_i = \int_{\Omega} \varphi_i^2(\xi)\, \xi, \tag{25–27}$$

δ_{ij} is the Kronecker delta, $\tilde{q}_i = (q_i - \bar{q}_i)$ is the zero-mean response of the ith generalized coordinate, with $\bar{q}_i$ being its mean. The norm of the basis functions τ_i in the present case is $\pi RL/2$

for asymmetric modes and πRL for axisymmetric modes; without effect on the results, they can be assumed to be 0.5 and 1, respectively. In Eq. (24), **A** and **B** are symmetric and positive definite matrices of dimension $K \times K$, and $\boldsymbol{\alpha}$ is a vector containing the K unknown coefficients of the POM. The eigenvectors $\boldsymbol{\alpha}$ corresponding to the largest eigenvalues (known as dominant POM) in Eq. (24) can now be inserted in Eq. (23) that gives a basis for the approximate solution of the PDE using the Galerkin approach; this will be referred to as the POD-Galerkin scheme hereafter. The optimal number of terms $\tilde{K}$ to be retained can be estimated by $\sum_{i=1}^{\tilde{K}} \lambda_i / \sum_{i=1}^{K} \lambda_i \geqslant 0.99$ in Eq. (24); however, for each problem this cut-off value can be different. It would be useful to check the convergence of the solution by increasing the value $\tilde{K}$; over a certain value, the results can become less accurate, because the additional terms introduced in the expansion may be highly noise-polluted.

In some applications, it may be better to use time responses obtained for different system parameters in order to produce better POM.

By using Eqs. (10), (20) and (23), the expansion used for the POD solution is given by

$$w(\xi, t) = \sum_{i=1}^{\tilde{K}} a_i(t) \sum_{j=1}^{K} \alpha_{j,i} \varphi_j(\xi) = \sum_{i=1}^{\tilde{K}} a_i(t) \sum_{m=1}^{M} \sum_{n=0}^{N} \left[\alpha_{m,n,i} \cos(n\theta) + \beta_{m,n,i} \sin(n\theta)\right] \sin(\lambda_m x), \quad (28)$$

where on the right-hand side two different symbols, $\alpha_{m,n,i}$ and $\beta_{m,n,i}$, have been introduced to differentiate the coefficients of the POM for cosine and sine terms in θ and are given by the corresponding $\alpha_{j,i}$. Eq. (28) is used to solve Eqs. (1) and (3) with the Galerkin method to find the equations of motion of the reduced-order model. Moreover, Eq. (28) has still the same shape over the shell surface Eq. (18); therefore, the fluid–structure interaction can be treated with the same approach used for the Galerkin method. This is not surprising, because the POD modes have been projected on the eigenmodes. Details on the mathematics are given in Ref. [17].

4. Numerical results

The same water-filled circular cylindrical shell (without imperfections) investigated in Ref. [17] is considered, with the following dimensions and material properties: $L = 520\,\text{mm}$, $R = 149.4\,\text{mm}$, $h = 0.519\,\text{mm}$, $E = 2.06 \times 10^{11}\,\text{Pa}$, $\rho = 7800\,\text{kg/m}^3$, $\rho_F = 1000\,\text{kg/m}^3$ and $\nu = 0.3$. Numerical calculations have been performed for the fundamental mode ($n = 5$, $m = 1$) of the water-filled shell, a case previously studied by Amabili [8]. The natural frequency $\omega_{1,n}$ of this mode is 79.21 Hz, according to Donnell's theory of shells; modal damping $\zeta_{1,n} = 0.0017$ is assumed.

The response–frequency relationship of the fundamental mode of the perfect, water-filled shell under harmonic point excitation of magnitude 3 N at $\tilde{x} = L/2$ and $\tilde{\theta} = 0$ is given in Fig. 2. Responses obtained by using the conventional Galerkin approach with 16 dofs and by using three POM compare very well. This result has been obtained by choosing the best of a few POD models developed in Ref. [17]. This POD model has been built by using the quasi-periodic time response with modulations of amplitude for $\omega/\omega_{1,n} = 0.991$ on branch "2", where both driven and companion modes are active. Both travelling waves around the shell in opposite directions have been taken into account (one obtained by direct integration and the other by changing the sign to the generalized coordinates associated to $\sin(n\theta)$ terms in Eq. (10b)) to construct the POD

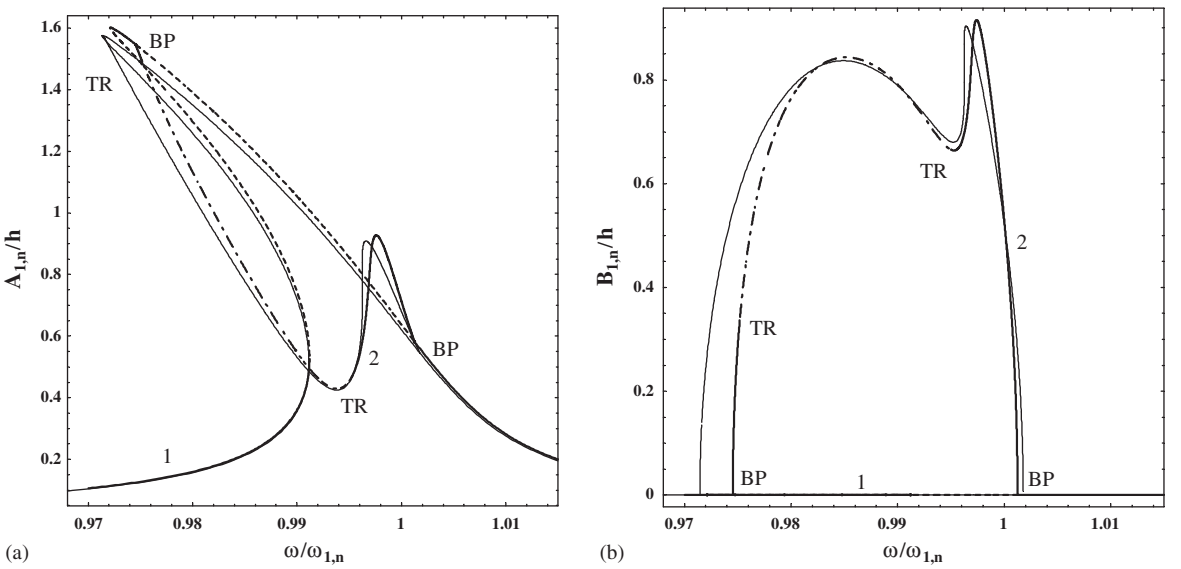

Fig. 2. Maximum amplitude of vibration versus excitation frequency; POD model with three modes ($\omega/\omega_{1,n} = 0.991$) versus the conventional Galerkin model. (a) Maximum amplitude of $A_{1,n}(t)$, driven mode; (b) maximum amplitude of $B_{1,n}(t)$, companion mode; 1, branch "1"; 2, branch "2"; BP, pitchfork bifurcation; TR, Neimark–Sacker (torus) bifurcations. ——, conventional Galerkin model; ▬▬, POD model, stable periodic solutions (three modes from quasi-periodic response); ▬·▬, POD model, stable quasi-periodic solutions; ▬ ▬, POD model, unstable periodic solutions.

reduced-order model. It should be observed that the natural frequency computed with this POD reduced-order model is practically identical to the one computed with the conventional model.

Fig. 2 shows the main branch "1" corresponding to zero amplitude of the companion mode $B_{1,n}(t)$; this branch has pitchfork bifurcations (BP) at $\omega/\omega_{1,n} = 0.9714$ and at 1.0018, where branch "2" appears. This new branch corresponds to participation of both $A_{1,n}(t)$ and $B_{1,n}(t)$, giving a travelling wave response. Branch "2" undergoes two Neimark–Sacker (torus) bifurcations (TR), at $\omega/\omega_{1,n} = 0.9716$ and 0.9949. Amplitude-modulated (quasiperiodic) response is indicated in Fig. 2 for $0.9716 < \omega/\omega_{1,n} < 0.9949$, i.e. bracketed by the two Neimark–Sacker bifurcations.

The optimal number of POM $\tilde{K}$ to be retained in the reduced-order model can be estimated by plotting $\sum_{i=1}^{\tilde{K}} \lambda_i / \sum_{i=1}^{K} \lambda_i$ as a function of $\tilde{K}$, as has been done in Fig. 3 for the reduced model extracted from a quasi-periodic response. This figure clearly indicates that three proper orthogonal modes absorb practically all of the shell energy for the response at $\omega/\omega_{1,n} = 0.991$. The coefficients of the main proper orthogonal modes, to be inserted in Eq. (33), are given in Table 1. The first is the driven mode, the second is the companion mode and the third is the axisymmetric mode.

Poincaré maps have been computed by direct integration of the equations of motion. The excitation frequency ω has been kept constant, $\omega = 0.92\,\omega_{1,n}$ (the shell displays softening-type response; therefore, for large excitation, the resonance is obtained for $\omega < \omega_{1,n}$), and the excitation amplitude has been varied between 0 and 600 N. The force range has been divided into 500 steps, so that the force is varied in steps of 1.2 N. Each time the force is changed by a step, 500 periods

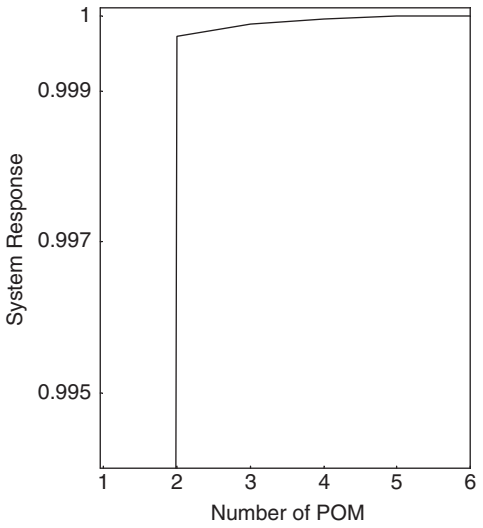

Fig. 3. Significance of POD eigenvalues versus the number of POM; POM extracted from quasi-periodic response.

Table 1
Coefficients of the main POM

Time response	ith POM	$\alpha_{1,5,i}$	$\beta_{1,5,i}$	$\alpha_{1,10,i}$	$\beta_{1,10,i}$	$\alpha_{1,0,i}$	$\alpha_{3,0,i}$
$\omega/\omega_{1,n} = 0.991$	1	1	0	0.000213	0	0.0000434	8.85×10^{-6}
	2	0	1	0	−0.000291	0	0
	3	0.000123	0	−0.1847	0	−0.9641	0.1855
Chaotic response 550 N ($\omega/\omega_{1,n} = 0.92$)	1	1	0	0.0006039	0	−0.009812	0.002283
	2	0	1	0	−0.000273	0	0
	3	−0.02058	0	0.009702	0	−0.9914	0.1143
	4	0	−0.000873	0	0.9975	0	0
	5	−0.001390	0	−0.9965	0	−0.003704	0.009041

have been allowed to elapse in order to eliminate the transient motion. The initial condition at the first step is zero displacement and velocity for all the variables; in the following steps, the solution at the previous step, with addition of a small perturbation in order to find a stable solution, is used as initial condition. The bifurcation diagrams obtained by all these Poincaré maps by using the conventional Galerkin model are shown in Figs. 4 and 5. In particular, in Fig. 4 the load is increased from 0 to 600 N; in Fig. 5 the load is decreased from 600 N to 0. Simple periodic motion, a period-doubling bifurcation, subharmonic response, amplitude modulations and chaotic response have been detected, as shown in Figs. 4(a, b) and 5(a, b). This indicates the existence of complex nonlinear dynamics for the circular cylindrical shell subject to large harmonic excitation. Comparison of Figs. 4 and 5, where only stable solutions are reported, shows that only in some regions the shell exhibits the same behaviour when the load (bifurcation parameter) is increased or

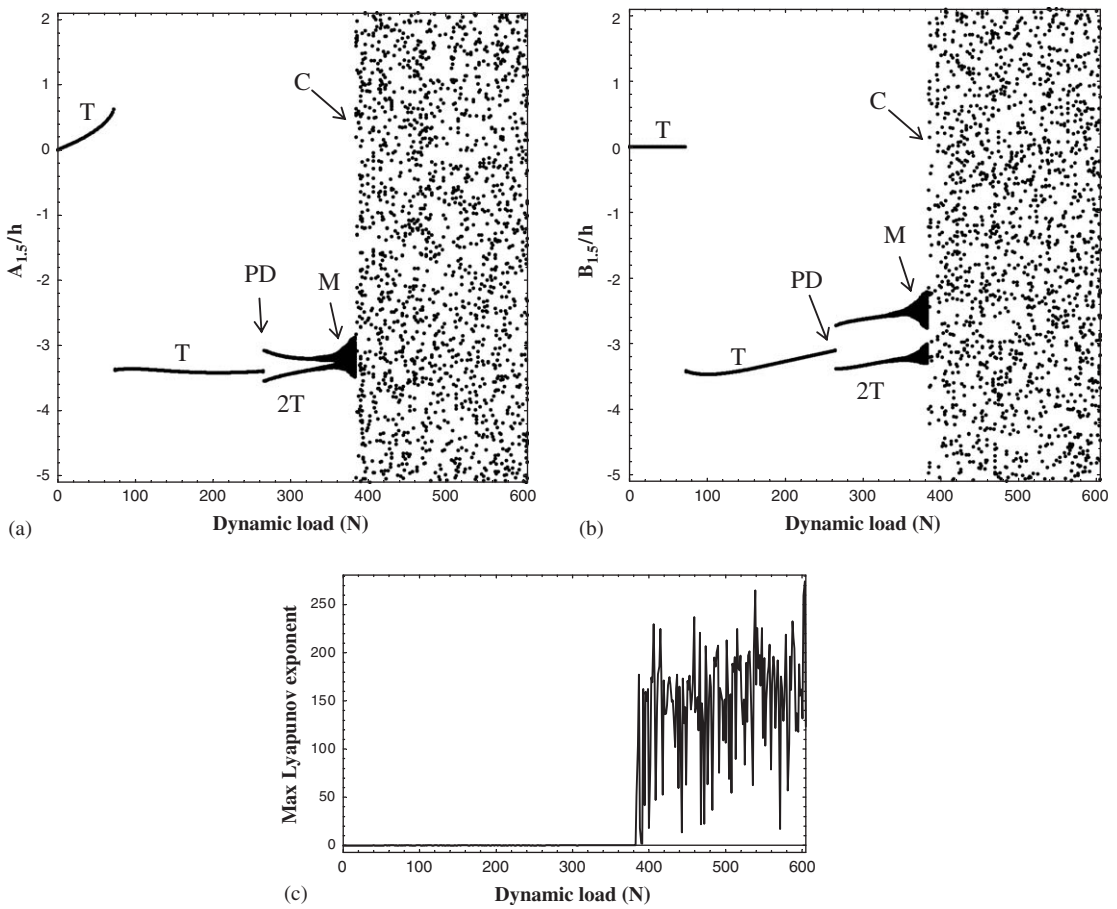

Fig. 4. Bifurcation diagram of Poincaré maps and maximum Lyapunov exponent for the shell under increasing harmonic load with frequency $\omega = 0.92\omega_{1,n}$; conventional Galerkin model, 16 dofs. (a) Generalized coordinate $A_{1,n}(t)$, driven mode; T = response period equal to excitation period; PD = period doubling bifurcation; 2T = periodic response with two times the excitation period; M = amplitude modulations; C = chaos; (b) generalized coordinate $B_{1,n}(t)$, companion mode; (c) maximum Lyapunov exponent.

decreased. This indicates that different stable solutions coexist for the same set of system parameters, so that the solution is largely affected by initial conditions.

Figs. 4(c) and 5(c) give the maximum Lyapunov exponent σ_1 associated with the bifurcation diagram. It can be observed that (i) for periodic forced vibrations, $\sigma_1 < 0$, (ii) for quasi-periodic response, $\sigma_1 = 0$ and (iii) for chaotic response, $\sigma_1 > 0$. Therefore, σ_1 can conveniently be used for identification of the system dynamics. Unfortunately the scale in Figs. 4(c) and 5(c) does not allow to distinguish $\sigma_1 < 0$ (around -0.13) from $\sigma_1 = 0$. It must be observed that books on chaos, see e.g. Ref. [20], generally report that σ_1 must be equal to zero for all trajectories not ending in a fixed point. This is correct for autonomous systems. In case of periodic forced vibrations, it is possible to introduce a dummy variable and transform our problem into an autonomous one. However, this operation is not useful because in this case σ_1 will be zero for both periodic and

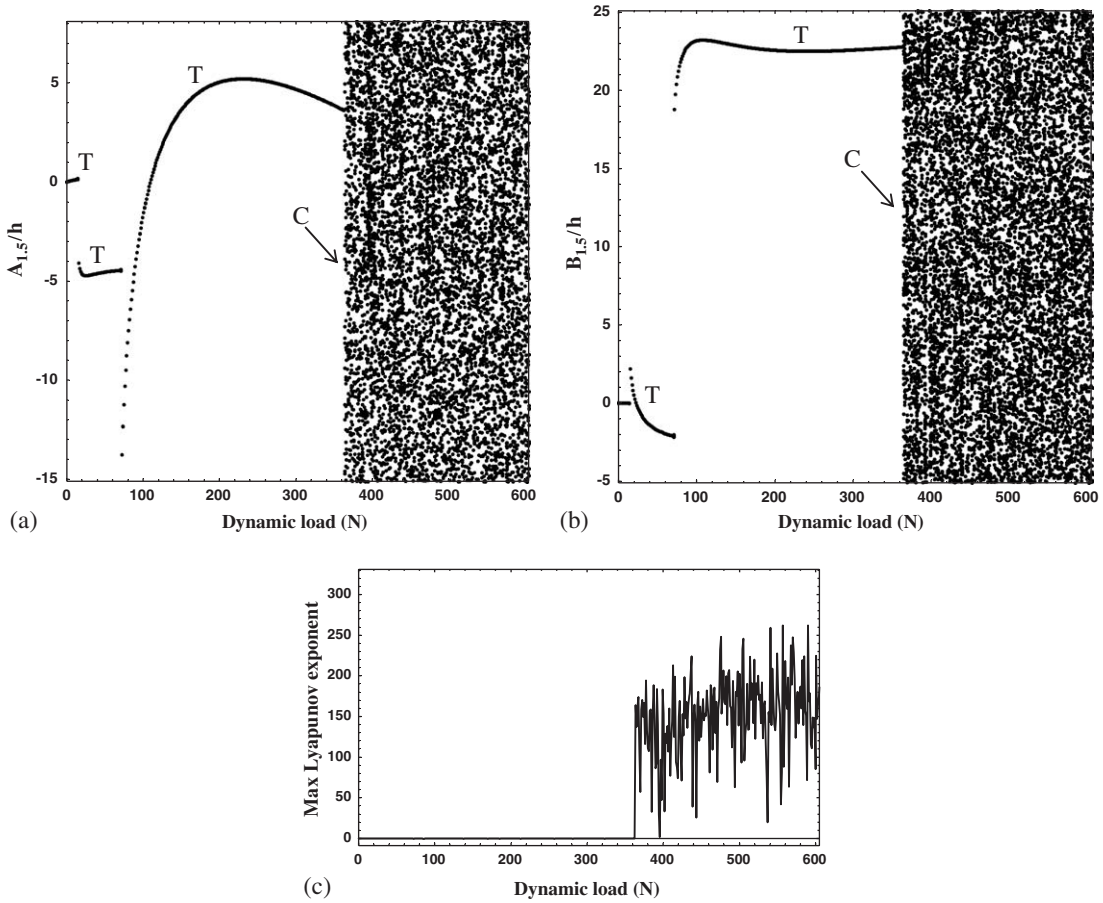

Fig. 5. Bifurcation diagram of Poincaré maps and maximum Lyapunov exponent for the shell under decreasing harmonic load with frequency $\omega = 0.92\omega_{1,n}$; conventional Galerkin model, 16 dofs. (a) Generalized coordinate $A_{1,n}(t)$, driven mode; T = response period equal to excitation period; C = chaos; (b) generalized coordinate $B_{1,n}(t)$, companion mode; (c) maximum Lyapunov exponent; (d) 3-D representation of the bifurcation diagram: generalized coordinate $A_{1,n}(t)$, enlarged scale.

quasi-periodic response. It is more interesting to compute the maximum Lyapunov exponent of the non-autonomous system and use the classification previously reported, which cannot be found in books. The physical reason for $\sigma_1 < 0$ for periodic response of the non-autonomous forced system is that any perturbation of displacement or velocity is damped; in fact, a perturbation in the direction of the trajectory in the phase space will be cancelled because it changes the phase relationship between excitation and response. This is the difference with respect to an autonomous system, for which a perturbation in the direction of the trajectory will stay, giving $\sigma_1 = 0$.

Figs. 4 and 5 can be compared to the analogous Figs. 6 and 7, respectively, computed with the reduced-order model obtained by using three POM from the quasi-periodic time response at $\omega/\omega_{1,n} = 0.991$ and excitation of magnitude 3 N. Comparison of the results is not bad, especially considering that the POM used in the reduced-order model have been extracted for a small

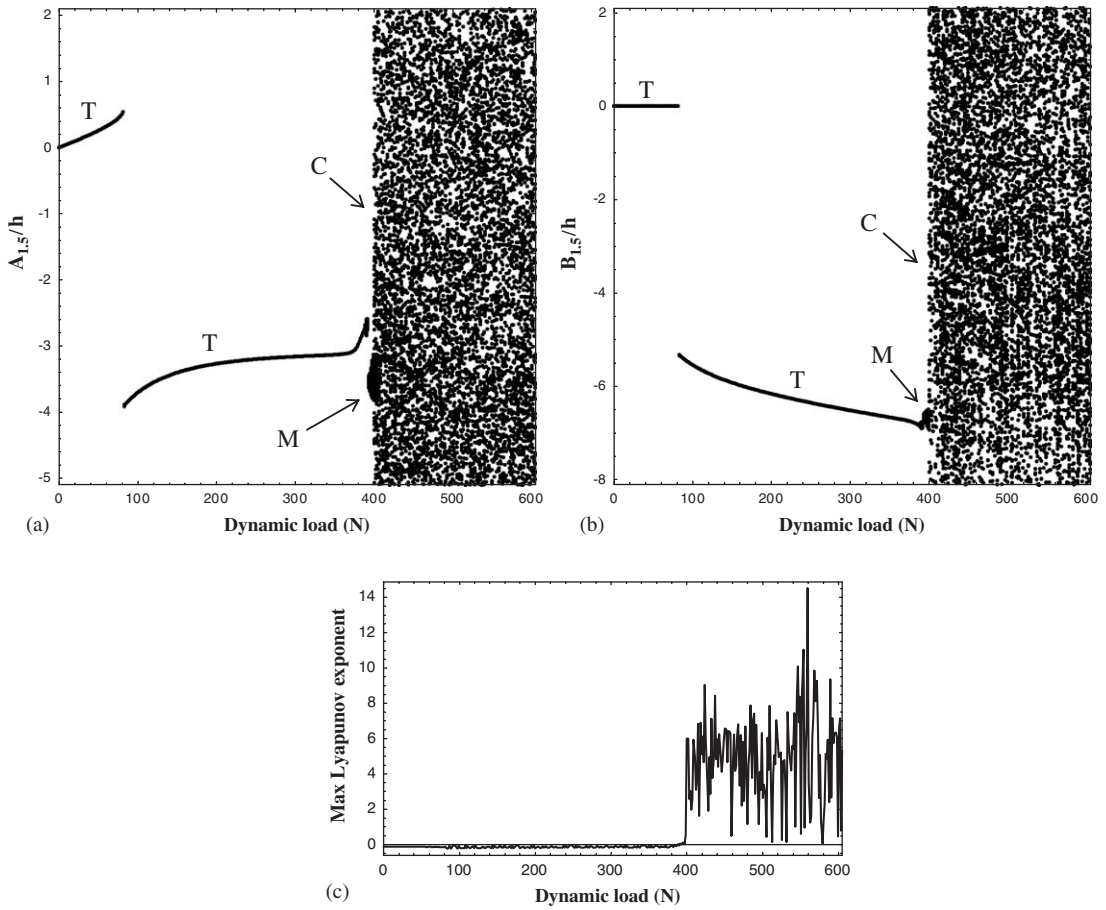

Fig. 6. Bifurcation diagram of Poincaré maps and maximum Lyapunov exponent for the shell under increasing harmonic load with frequency $\omega = 0.92\omega_{1,n}$; reduced-order model with three POM from quasi-periodic response. (a) Generalized coordinate $A_{1,n}(t)$, driven mode; T = response period equal to excitation period; M = amplitude modulations; C = chaos; (b) generalized coordinate $B_{1,n}(t)$, companion mode; (c) maximum Lyapunov exponent.

excitation magnitude (3 N) in relation to the maximum magnitude (600 N) reached in the bifurcation diagrams and for a different excitation frequency ($\omega/\omega_{1,n} = 0.991$ instead of $\omega/\omega_{1,n} = 0.92$). In particular, Figs. 4 and 6 show a similar threshold for the onset of chaotic response and a similar initial jump in the periodic response. However, a large difference in the maximum Lyapunov exponent of the chaotic response indicates that in the reduced-order model the system displays a lower-dimensional chaos than in the original 16-dof model. Moreover, the period-doubling bifurcation is not detected in the reduced-order model. Similar differences, especially in the chaotic region, are detected when comparing Figs. 5 and 7.

The effect of adding two additional POM to the reduced-order model (i.e. with a total of five POM) is investigated in Fig. 8. It is seen that these additional modes give poor results and greatly decrease the accuracy of the model. In fact, as indicated in Fig. 3, additional POM extracted from the quasi-periodic time response at $\omega/\omega_{1,n} = 0.991$ are associated with practically zero energy and

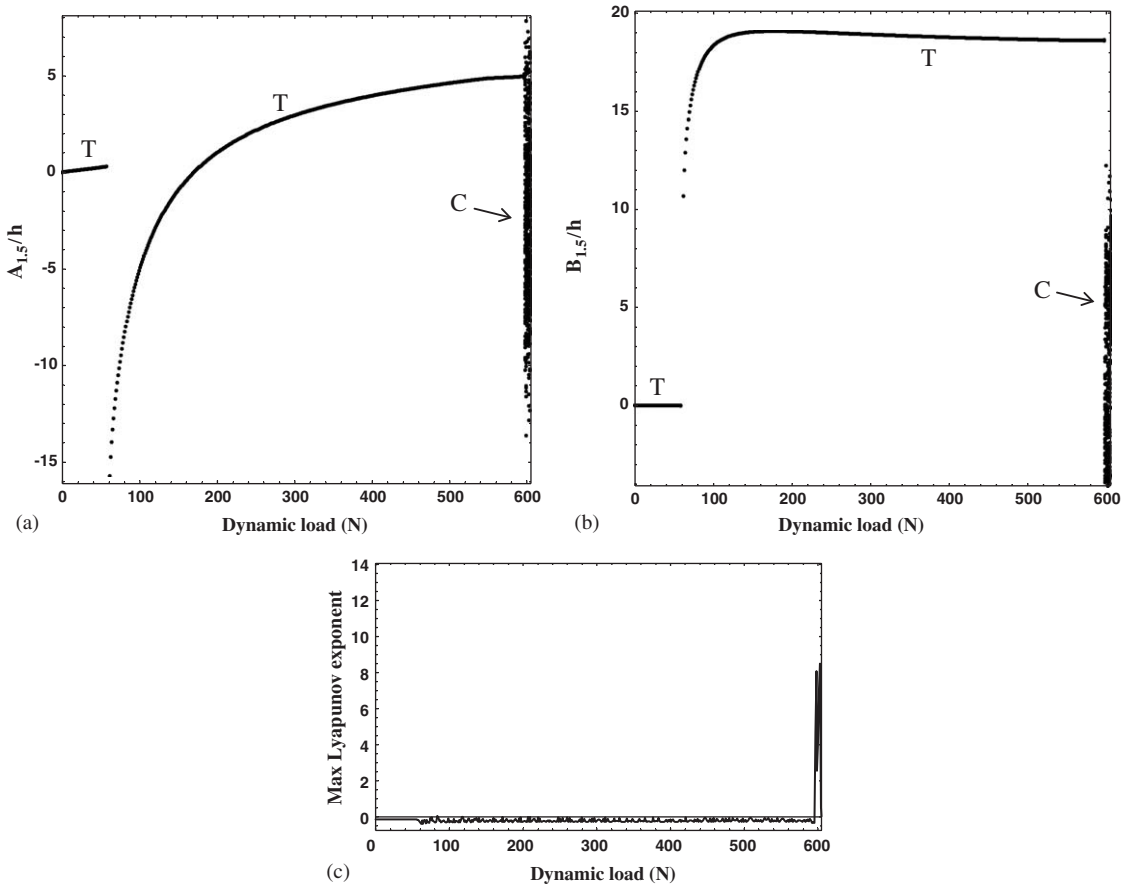

Fig. 7. Bifurcation diagram of Poincaré maps and maximum Lyapunov exponent for the shell under decreasing harmonic load with frequency $\omega = 0.92\omega_{1,n}$; reduced-order model with three POM from quasi-periodic response. (a) Generalized coordinate $A_{1,n}(t)$, driven mode; T = response period equal to excitation period; C = chaos; (b) generalized coordinate $B_{1,n}(t)$, companion mode; (c) maximum Lyapunov exponent.

therefore are highly noise-polluted. Therefore, no improved model (vis-à-vis the one with three modes) can be obtained by using a POD extracted from the quasi-periodic time response at $\omega/\omega_{1,n} = 0.991$ and excitation of magnitude 3 N.

4.1. POM extracted from chaotic response

The time response computed with the conventional Galerkin model with 16 dofs for $\omega/\omega_{1,n} = 0.92$ and excitation of magnitude 550 N is given in Fig. 9 for the most significant generalized coordinates. As previously indicated in Fig. 4 for a dynamic load of 550 N, this response is chaotic. This time response has been used to extract POM; also, in this case, travelling waves in opposite directions have been considered. Fig. 10 shows the energy associated with the POD modes extracted. If compared to the analogous Fig. 3, in this case more modes are necessary to

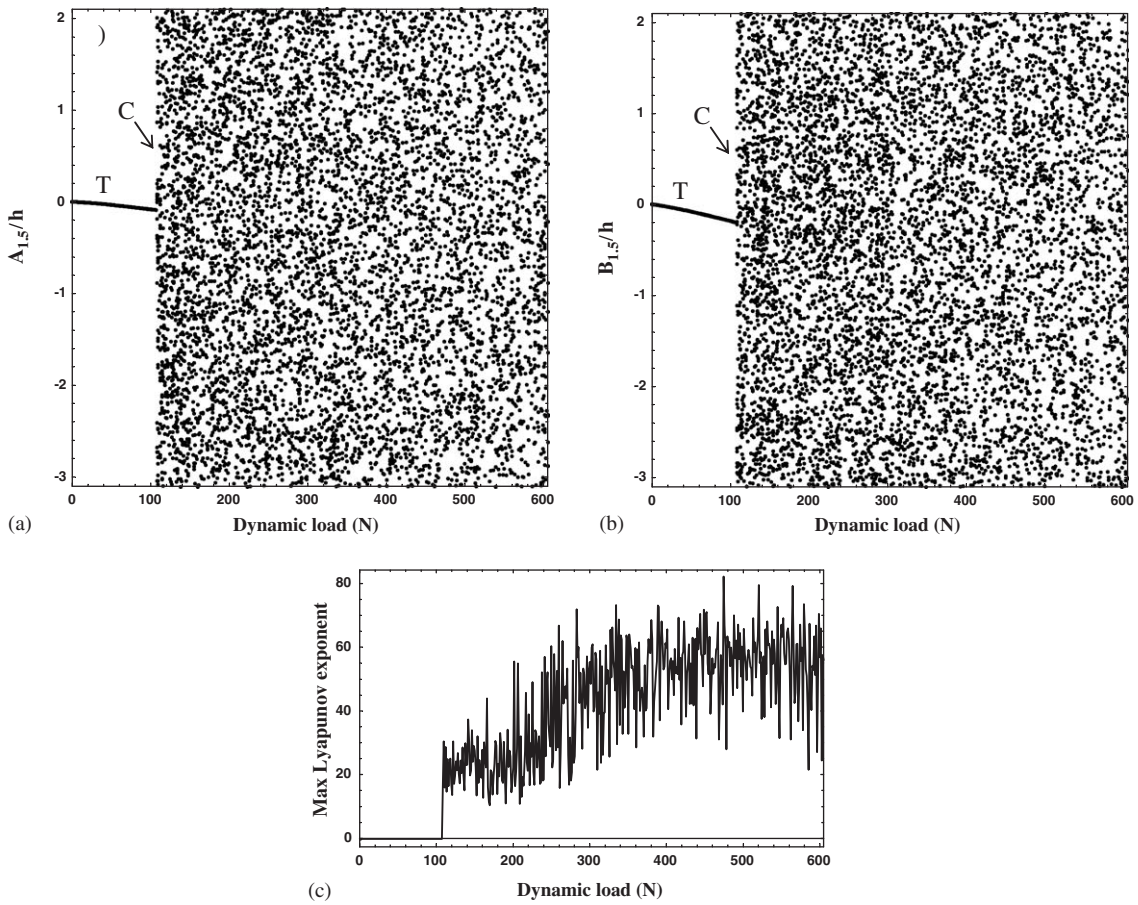

Fig. 8. Bifurcation diagram of Poincaré maps and maximum Lyapunov exponent for the shell under increasing harmonic load with frequency $\omega = 0.92\omega_{1,n}$; reduced-order model with five POM from quasi-periodic response. (a) Generalized coordinate $A_{1,n}(t)$, driven mode; T = response period equal to excitation period; C = chaos; (b) generalized coordinate $B_{1,n}(t)$, companion mode; (c) maximum Lyapunov exponent.

reach convergence to the global shell energy. Specifically, complete convergence is reached only with 16 modes, i.e. with no reduction in the order of the model! However, with three modes, more than 90% of the energy is captured and, with five modes, about 96%. It must be pointed out that convergence of the Galerkin solution in the chaotic regime has not been verified.

The coefficients of the main POM, to be inserted in Eq. (33), are given in Table 1 and can be compared to those obtained from quasi-periodic response. It can be observed that the first two POM are almost identical, but the third one, that is practically an axisymmetric mode, has a different coefficient for the third axisymmetric term $\alpha_{3,0,3}$. It must be pointed out that, in this case, the reduced-order models display non-negligible linear coupling of the equations of motion and different natural frequencies with respect to the conventional Galerkin model, i.e. $\omega_{1,n} = 80.81$ (model with three modes) and 80.78 Hz (model with five modes). In particular, for these reduced order models it has been found that better results are obtained by non-dimensionalizing the

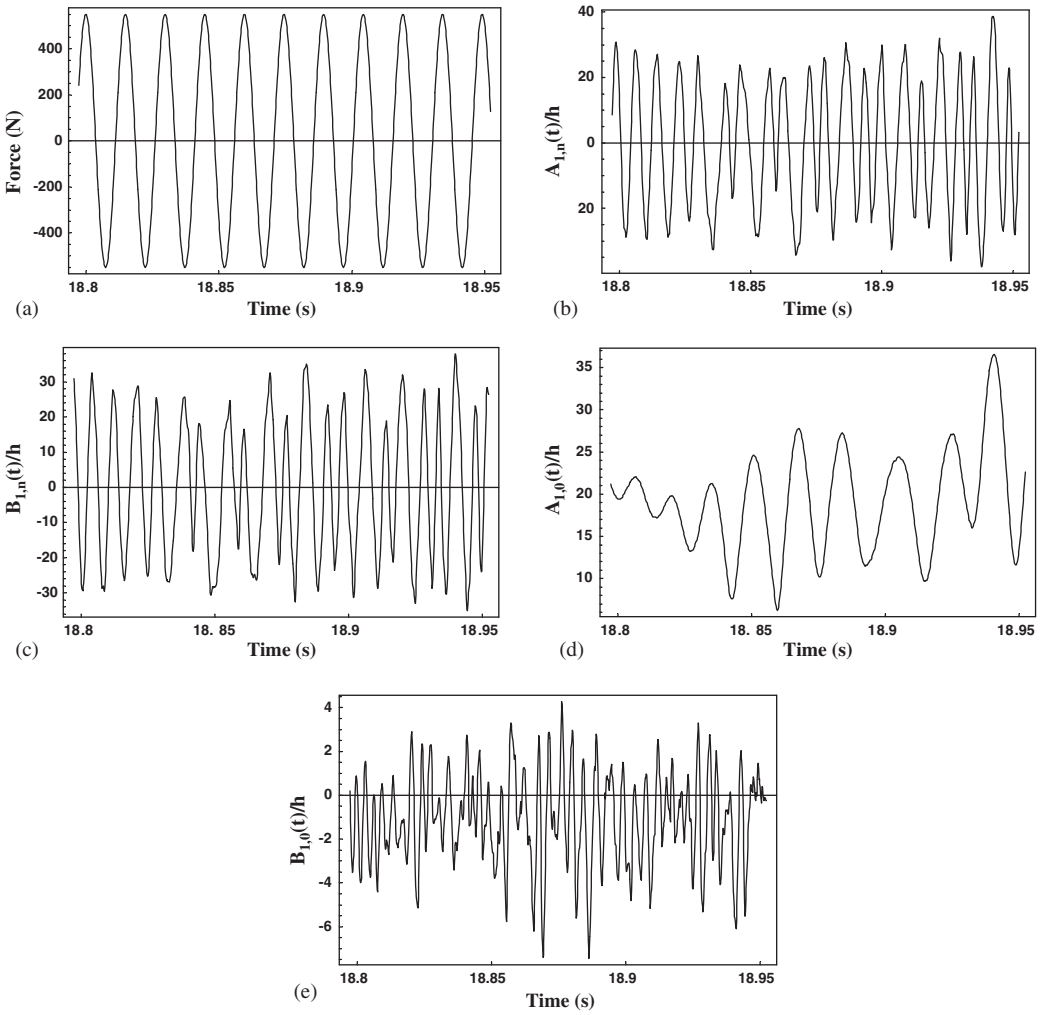

Fig. 9. Chaotic time response at excitation frequency $\omega/\omega_{1,n} = 0.92$ and excitation of 550 N; conventional Galerkin model, 16 dofs. (a) Harmonic force excitation; (b) modal coordinate $A_{1,n}(t)$ associated to the driven mode; (c) modal coordinate $B_{1,n}(t)$ associated to the companion mode; (d) modal coordinate $A_{1,0}(t)$ associated to the first axisymmetric mode; (e) modal coordinate $A_{3,0}(t)$ associated to the third axisymmetric mode.

equations with respect to $\omega_{1,n} = 85.29$ Hz, which is the linear frequency computed neglecting linear coupling of the equations.

The reduced-order model with three POM extracted from a chaotic response gives the bifurcation diagram shown in Fig. 11. Comparison of Fig. 4 (original Galerkin model), Fig. 6 (model with three POM extracted from quasi-periodic response) and Fig. 11 indicates that the reduced model with three modes constructed from the chaotic response is not accurate. Fig. 11(c) shows a maximum Lyapunov exponent around four in the chaotic region instead of 180 obtained with the original Galerkin model; this figure shows that the maximum Lyapunov exponent can be

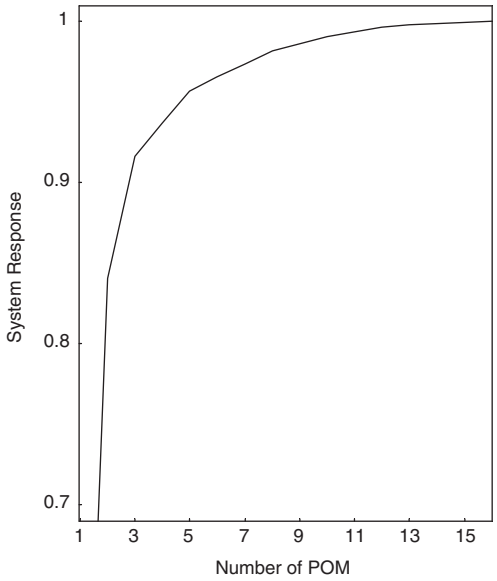

Fig. 10. Significance of POD eigenvalues versus the number of proper orthogonal modes (POM); POM extracted from chaotic response.

used to classify periodic and quasi-periodic motion, as previously discussed in Section 4. The reason for this poor result is that three modes do not reach energy convergence, as indicated by Fig. 10. Therefore, a second model with five POM has been built. Bifurcation diagrams increasing and decreasing the excitation are presented in Figs. 12 and 13, respectively. They show a large improvement of the accuracy of the model with respect to Fig. 11. In particular, comparison of Fig. 4 (original model) and Fig. 12 shows an different initial jump for relatively small excitation, but then the shell behaviour with the period-doubling bifurcation and onset of chaos are reproduced with accuracy. A periodic solution in Fig. 12 appears after a range of chaotic response; this is different to Fig. 4. However, it must be observed that, in this range of excitation, more solutions (periodic and chaotic) coexist, so it is possible to find some differences in the bifurcation diagrams even with small differences in the step used to vary the excitation magnitude. In fact, depending on the initial conditions for each computation step, either a periodic or a chaotic solution may be obtained. It is also interesting to observe that the maximum Lyapunov exponent in the chaotic region in Fig. 12 reaches almost the magnitude of the one obtained in Fig. 4. Comparison of Figs. 5 and 13 shows similar analogies.

Poincaré maps obtained from zero initial conditions for $\omega/\omega_{1,n} = 0.92$ and excitation of magnitude 550 N with the conventional Galerkin method with 16 modes and the reduced model with five modes obtained from the chaotic response are shown in Figs. 14 and 15, respectively. The results cover the same region of the plane, with a relatively small difference in the shape of the chaotic attractor. In particular, Fig. 15 shows a chaotic behaviour in contrast to Figs. 12 and 13 for a load of 550 N that show periodic response. As previously discussed, in this region more solutions (periodic and chaotic) coexist. All the Lyapunov exponents in this case have been

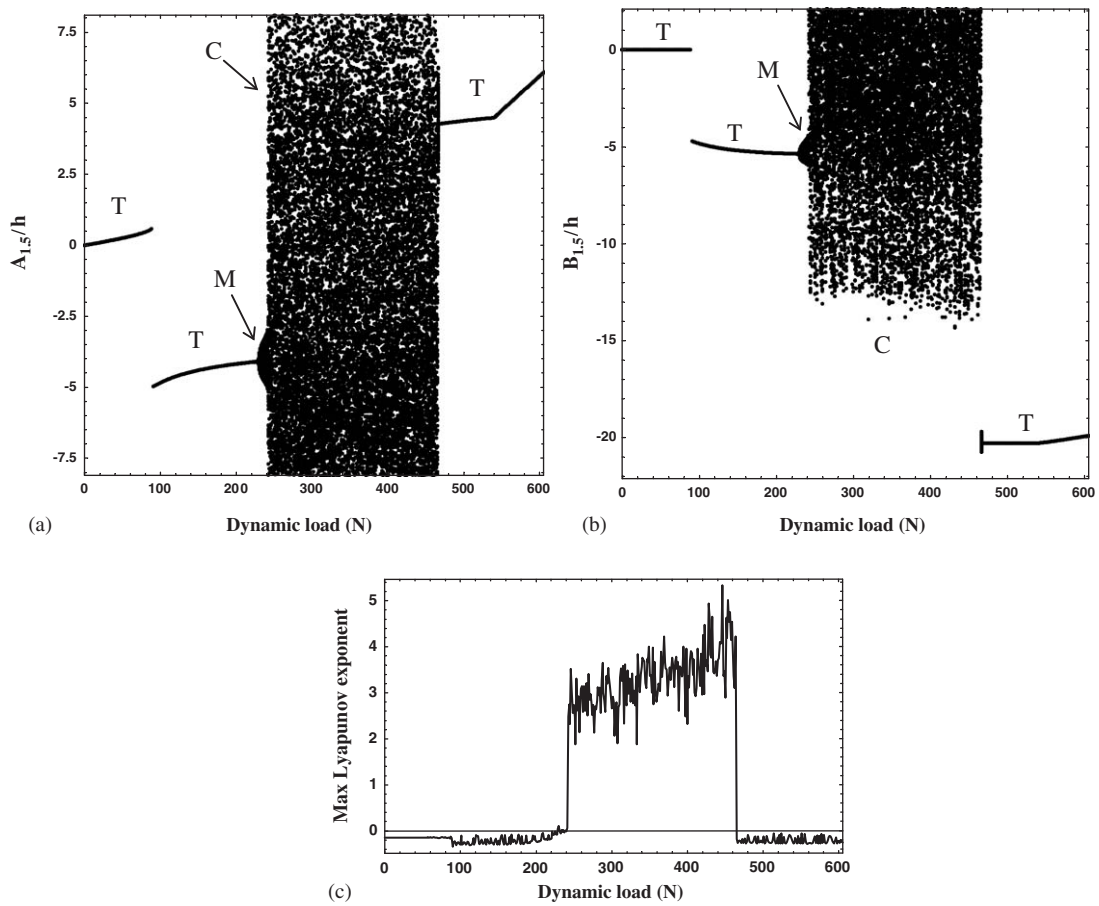

Fig. 11. Bifurcation diagram of Poincaré maps and maximum Lyapunov exponent for the shell under increasing harmonic load with frequency $\omega = 0.92\,\omega_{1,n}$; reduced-order model with three POM from chaotic response. (a) Generalized coordinate $A_{1,n}(t)$, driven mode; T = response period equal to excitation period; M = amplitude modulations; C = chaos; (b) generalized coordinate $B_{1,n}(t)$, companion mode; (c) maximum Lyapunov exponent.

computed for the conventional Galerkin model (16 dofs) and the reduced POD model with five modes from the chaotic response; these exponents are given in Tables 2 and 3 respectively. From Table 2 it is evident that the response is associated with hyperchaos with 16 positive Lyapunov exponents, which is a very high-dimensional chaos, as indicated by the Lyapunov dimension, which is 31.8. Such a large number of positive Lyapunov exponents for chaotic behaviour of a structure (in the present model the fluid gives only an added inertia) do not seem to have been reported in the literature before. This indicates that the 16-dof model is already at its limit for describing the chaotic response. For this reason, it is impossible to pretend in this case that the reduced order model with only 5 dofs is fully accurate, for the chaotic regime. The reduced order model has five positive Lyapunov exponents and a Lyapunov dimension 9.96.

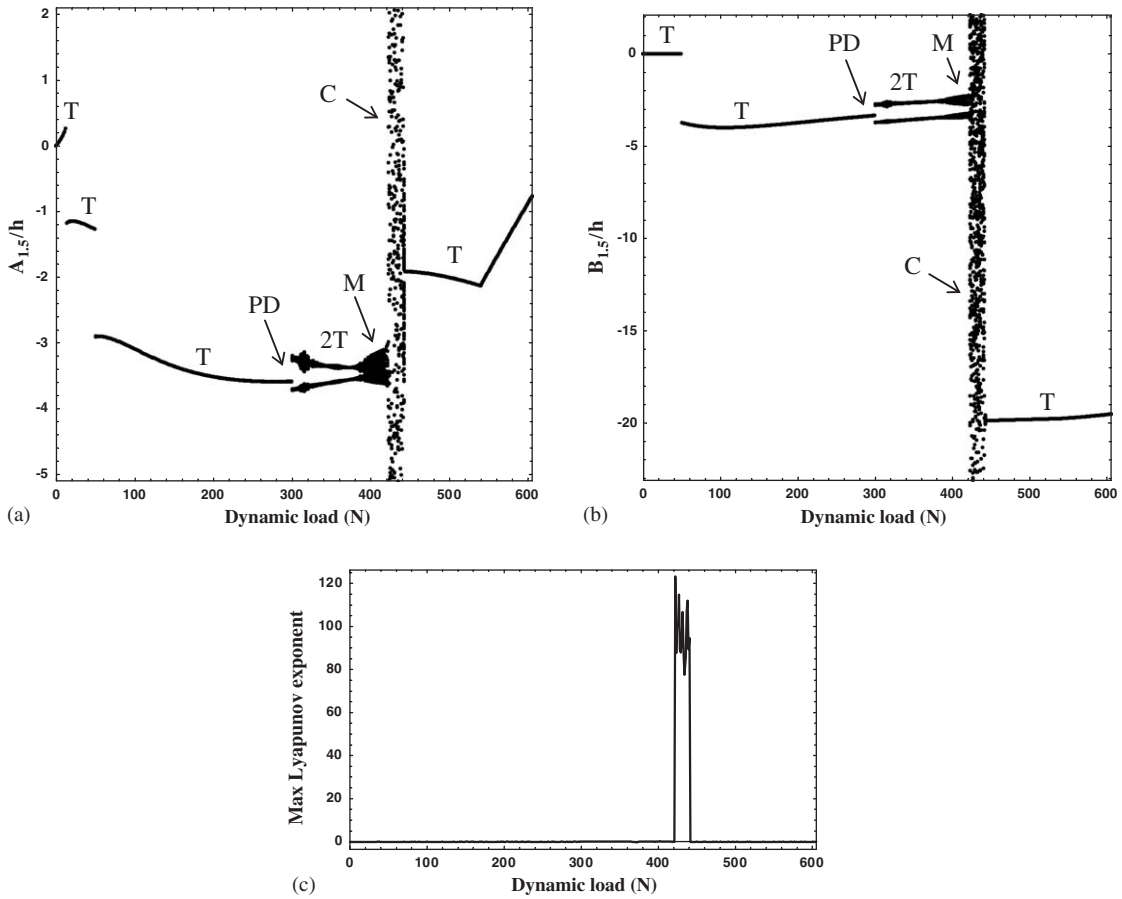

Fig. 12. Bifurcation diagram of Poincaré maps and maximum Lyapunov exponent for the shell under increasing harmonic load with frequency $\omega = 0.92\omega_{1,n}$; reduced-order model with five POM from chaotic response. (a) Generalized coordinate $A_{1,n}(t)$, driven mode; T = response period equal to excitation period; PD = period doubling bifurcation; 2T = periodic response with two times the excitation period; M = amplitude modulations; C = chaos; (b) generalized coordinate $B_{1,n}(t)$, companion mode; (c) maximum Lyapunov exponent.

5. Conclusions

Complex nonlinear dynamics of a water-filled circular cylindrical shell has been accurately studied by using initially a Galerkin solution with 16 dofs. By using bifurcation diagrams, Poincaré maps, time responses, Lyapunov exponents and Lyapunov dimensions, the following phenomena have been observed: (i) a period-doubling bifurcation, (ii) subharmonic response, (iii) quasi-periodic response and (iv) chaotic behaviour with up to 16 positive Lyapunov exponents (hyperchaos).

Results for large-amplitude vibrations of a shell show that a sufficiently accurate reduced-order POD model capable of describing very large variations of the system parameters, where regular

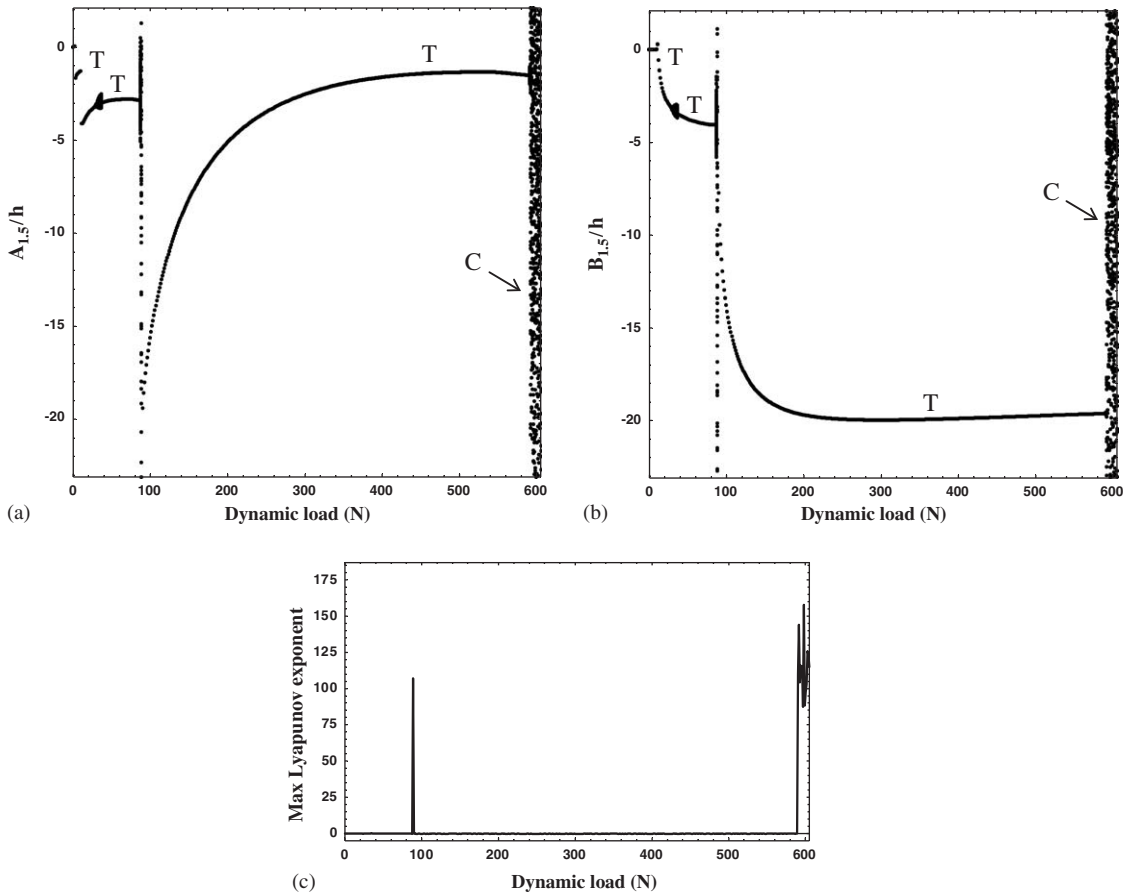

Fig. 13. Bifurcation diagram of Poincaré maps and maximum Lyapunov exponent for the shell under decreasing harmonic load with frequency $\omega = 0.92\omega_{1,n}$; reduced-order model with five POM from chaotic response. (a) Generalized coordinate $A_{1,n}(t)$, driven mode; T = response period equal to excitation period; C = chaos; (b) generalized coordinate $B_{1,n}(t)$, companion mode; (c) maximum Lyapunov exponent.

and chaotic responses are observed, can be built by using chaotic response time series. In fact, more POM are necessary to reach energy convergence using time series extracted from chaotic response than from the quasi-periodic or periodic responses. Therefore, if chaotic responses are used, then more POD modes associated with significant energy can be extracted than if regular responses are used. The addition of POM associated with very small energy diminishes the accuracy achieved by the reduced-order model. However, reduced models with more POM associated with significant energy are more suitable to describe large variations of the system parameters, i.e. large variations of the excitation magnitude in the present study. It must also be observed that it is necessary to utilize both of the mirror-image responses, involving travelling waves in opposite directions.

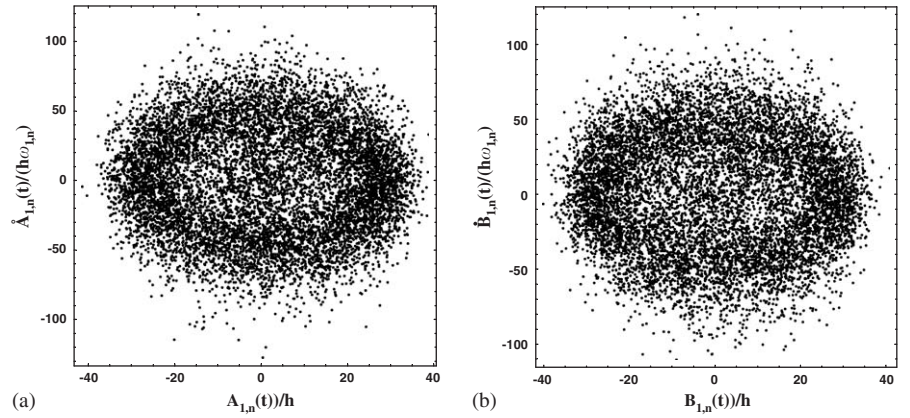

Fig. 14. Poincaré map for the shell under harmonic load with frequency $\omega = 0.92\omega_{1,n}$ and magnitude 550 N; conventional Galerkin model, 16 dofs. (a) Generalized coordinate $A_{1,n}(t)$, driven mode; (b) generalized coordinate $B_{1,n}(t)$, companion mode.

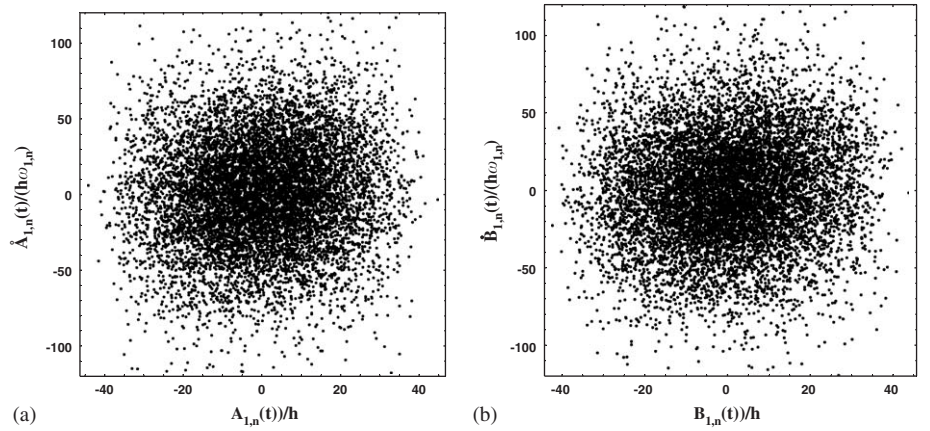

Fig. 15. Poincaré map for the shell under harmonic load with frequency $\omega = 0.92\omega_{1,n}$ and magnitude 550 N; reduced-order model with five POM from chaotic response. (a) Generalized coordinate $A_{1,n}(t)$, driven mode; (b) generalized coordinate $A_{1,n}(t)$, companion mode.

Table 2
All the Lyapunov exponents for the shell under harmonic load with frequency $\omega = 0.92\omega_{1,n}$ and magnitude 550 N; conventional Galerkin model, 16 dofs

Positive Lyapunov exponents	Negative Lyapunov exponents
180.2, 150.4, 126.1, 106.4, 89.4, 73.6, 61.5, 51.8, 41.2, 32.2, 24.4, 16.7, 11.2, 6.61, 2.55, 0.35	−1.00, −4.30, −8.64, −13.7, −19.3, −27.0, −35.2, −43.6, −52.6, −64.3, −77.4, −91.8, −107.6, −128.6, −151.6, −183.1

Table 3
All the Lyapunov exponents for the shell under harmonic load with frequency $\omega = 0.92\omega_{1,n}$ and magnitude 550 N; reduced-order model with five POM from chaotic response

Positive Lyapunov exponents	Negative Lyapunov exponents
93.9, 40.1, 21.6, 9.1, 0.55	−1.5, −9.4, −22.5, −41.7, −94.3

In Section 4.1, reduced models have been stopped at five modes extracted from the chaotic response. Further addition of modes (up to eight modes has been tried) has not improved the results.

It may be opportune to offer here a few thoughts on the usefulness and efficacy of reduced-order POD methodology. There is no question, first of all, that POD reduced-order models are very useful in some realms, such as for aeroelasticity applications, in which model reductions from thousands and hundreds of dofs down to hundreds and tens, for the fluid and the structure, respectively, are routinely and usefully effected. This is especially true if many calculations are necessary, e.g. for optimization or fine-tuning a design, in which the parameters are not varied too far afield vis-à-vis those for which the POD model was constructed.

In some other applications, however, things are not straightforward: i.e., when the methodology of defining the dominant modes, constructing the POD model, and using it without further adjustment (e.g., as a result of less than satisfactory prediction, as compared to the dynamics obtained by the full model) breaks down. Indeed, there exist cases where the POD model is shown not to be optimal or even correct [24,25]. A case where considerable additional insight had to be brought to bear before a truly successful POD model could be constructed for cylindrical shell vibrations is that of Ref. [17]. Another case, involving a non-conservative fluid-conveying pipe system, shows that the POD model obtained can be used successfully over relatively large excursions of the flow velocity, but not of the fluid-to-structure mass parameter [26].

This has been the experience gained with the present paper as well. Moreover, if two system parameters are varied, e.g. frequency and amplitude of the excitation, especially in the case of frequency if a second resonance is approached, more difficulties should be expected to find a recipe to build a reduced-order POD model. Thus, the POD methodology is not as ''robust'' as, say, the Galerkin one, in that it cannot be used ''blindly'', even though following a set of defined rules, with success guaranteed in all conceivable cases. The POD method is a very useful one, but remains sensitive in its application, and therefore care must be exercised in its use.

Acknowledgements

This work was partially supported by the FIRB 2001 and COFIN 2003 grants of the Italian Ministry for University and Research (MIUR) and NSERC (Canada) and a Canada Research chair offered to A.S.

References

[1] M. Amabili, M.P. Païdoussis, Review of studies on geometrically nonlinear vibrations and dynamics of circular cylindrical shells and panels, with and without fluid–structure interaction, *Applied Mechanics Reviews* 56 (2003) 349–381.

[2] D.A. Evensen, Nonlinear flexural vibrations of thin-walled circular cylinders, NASA TN D-4090, 1967.

[3] E.H. Dowell, C.S. Ventres, Modal equations for the nonlinear flexural vibrations of a cylindrical shell, *International Journal of Solids and Structures* 4 (1968) 975–991.

[4] M. Amabili, F. Pellicano, M.P. Païdoussis, Non-linear dynamics and stability of circular cylindrical shells containing flowing fluid. Part I: stability, *Journal of Sound and Vibration* 225 (1999) 655–699.

[5] M. Amabili, F. Pellicano, M.P. Païdoussis, Non-linear dynamics and stability of circular cylindrical shells containing flowing fluid, Part II: large-amplitude vibrations without flow, *Journal of Sound and Vibration* 228 (1999) 1103–1124.

[6] M. Amabili, F. Pellicano, M.P. Païdoussis, Non-linear dynamics and stability of circular cylindrical shells containing flowing fluid. Part III: truncation effect without flow and experiments, *Journal of Sound and Vibration* 237 (2000) 617–640.

[7] M. Amabili, F. Pellicano, M.P. Païdoussis, Non-linear dynamics and stability of circular cylindrical shells containing flowing fluid. Part IV: large-amplitude vibrations with flow, *Journal of Sound and Vibration* 237 (2000) 641–666.

[8] M. Amabili, Theory and experiments for large-amplitude vibrations of empty and fluid-filled circular cylindrical shells with imperfections, *Journal of Sound and Vibration* 262 (2003) 921–975.

[9] M. Amabili, Comparison of shell theories for large-amplitude vibrations of circular cylindrical shells: Lagrangian approach, *Journal of Sound and Vibration* 264 (2003) 1091–1125.

[10] S.A. Zahorian, M. Rothenberg, Principal component analysis for low-redundancy encoding of speech spectra, *Journal of the Acoustical Society of America* 69 (1981) 519–524.

[11] L. Sirovich, Turbulence and dynamics of coherent structures, Part I: coherent structures, *Quarterly of Applied Mathematics* 45 (1987) 561–571.

[12] N. Aubry, P. Holmes, J.L. Lumley, E. Stone, The dynamics of coherent structures in the wall region of a turbulent boundary layer, *Journal of Fluid Mechanics* 192 (1988) 115–173.

[13] K.S. Breuer, L. Sirovich, The use of the Karhunen–Loève procedure for the calculation of linear eigenfunctions, *Journal of Computational Physics* 96 (1991) 277–296.

[14] M.F. Azeez, A.F. Vakakis, Proper orthogonal decomposition (POD) of a class of vibroimpact oscillations, *Journal of Sound and Vibration* 240 (2001) 859–889.

[15] A. Sarkar, M.P. Païdoussis, A compact limit-cycle oscillation model of a cantilever conveying fluid, *Journal of Fluids and Structures* 17 (2003) 525–539.

[16] G. Kerschen, B.F. Feeny, J.-C. Golinval, On the exploitation of chaos to build reduced-order models, *Computer Methods in Applied Mechanics and Engineering* 192 (2003) 1785–1795.

[17] M. Amabili, A. Sarkar, M.P. Païdoussis, Reduced-order models for nonlinear vibrations of cylindrical shells via the proper orthogonal decomposition method, *Journal of Fluids and Structures* 18 (2003) 227–250.

[18] S. Wolfram, *The Mathematica Book*, fourth edition, Cambridge University Press, Cambridge, UK, 1999.

[19] E.J. Doedel, A.R. Champneys, T.F. Fairgrieve, Y.A. Kuznetsov, B. Sandstede, X. Wang, AUTO 97: Continuation and Bifurcation Software for Ordinary Differential Equations (with HomCont), Concordia University, Montreal, Canada, 1998.

[20] J. Argyris, G. Faust, M. Haase, *An Exploration of Chaos*, North-Holland, Amsterdam, 1994.

[21] M. Amabili, Non-linear vibrations of doubly curved shallow shells, *International Journal of Non-Linear Mechanics* 40 (2005) 683–710.

[22] M.P. Païdoussis, *Fluid–Structure Interactions: Slender Structures and Axial Flow*, Vol. 2, Elsevier/Academic Press, London, UK, 2003.

[23] A. Sarkar, M.P. Païdoussis, A cantilever conveying fluid: coherent modes versus beam modes, *International Journal of Non-Linear Mechanics* 39 (2004) 467–481.

[24] J.P. Cusumano, B.Y. Bai, Period-infinity periodic motions, chaos, and spatial coherence of a 10 degree of freedom impact oscillator, *Chaos, Solitons and Fractals* 3 (1993) 515–535.
[25] J.P. Cusumano, D.C. Lin, Bifurcation and modal interaction in a simplified model of bending torsion vibrations of a thin elastica, *ASME Journal of Vibration and Acoustics* 117 (1995) 30–42.
[26] M.P. Païdoussis, A. Sarkar, C. Semler, A horizontal fluid-conveying cantilever: spatial coherent structures, beam modes and jumps in stability diagram, *Journal of Sound and Vibration* 280 (2005) 141–157.